Journal of Inflammation Research

Dovepress
Taylor & Francis Group

Open Access Full Text Article

ORIGINAL RESEARCH

Development of Diagnostic and Predictive Models for COPD Based on Anoikis Resistance

Wenmin Hu[1–3], Jingjing Sun[1–3], Mei Wang[1–3], Yaoyao Wang[2–4], Chaohui Mu[2,3], Xinjuan Yu[2,3], Peng Yuan[5], Wei Han[2,3], Yongchun Li[2,3,*], Qinghai Li[2,3,*]

[1]School of Medicine and Pharmacy, Ocean University of China, Qingdao, Shandong, 266071, People's Republic of China; [2]Qingdao Key Laboratory of Respiratory Comorbidity Remodeling and Precision Prevention, Qingdao Municipal Hospital, University of Health and Rehabilitation Sciences, Qingdao, 266071, People's Republic of China; [3]Department of Respiratory and Critical Care Medicine, Qingdao Municipal Hospital, University of Health and Rehabilitation Sciences, Qingdao, 266071, People's Republic of China; [4]Department of Respiratory and Critical Care Medicine, Qingdao Municipal Hospital, Qingdao University, Qingdao, 266071, People's Republic of China; [5]Department of General Practice, Qingdao Municipal Hospital, University of Health and Rehabilitation Sciences, Qingdao, 266071, People's Republic of China

*These authors contributed equally to this work

Correspondence: Yongchun Li; Qinghai Li, Email liych797@163.com; wflqh88@163.com

Journal of Inflammation Research downloaded from https://www.dovepress.com/
For personal use only.

Background: Chronic obstructive pulmonary disease (COPD) pathogenesis involves persistent airway inflammation and remodeling, yet the role of anoikis resistance remains poorly characterized. This study aimed to identify anoikis resistance-related hub genes and evaluate their clinical utility in COPD phenotyping and prognosis.

Methods: Integrated bioinformatics analysis of the GSE11906 dataset identified anoikis resistance-related differentially expressed genes (DEGs). Functional enrichment, LASSO regression, and machine learning (RF, SVM, XGB, GLM) were employed to pinpoint core hub genes. Multi-level validation included external datasets (GSE19407), in vitro (CSE-stimulated 16HBE cells), in vivo (cigarette smoke-exposed mice), and clinical samples (PBMCs). Diagnostic and prognostic models were developed using logistic regression.

Results: Five core hub genes (UCHL1, ME1, SLC2A1, BMP4, CRABP2) were identified, with ME1, SLC2A1, and BMP4 consistently upregulated in COPD across models and strongly correlated with emphysema index (negative, R = −0.41 to −0.45) and airway wall thickness (positive, R = 0.40–0.45). These genes exhibited significant associations with peribronchial immune cell infiltration. Diagnostic models for emphysema-predominant COPD (AUC = 0.860) and disease staging (AUC = 0.882), along with a prognostic model for hospitalization duration (AUC = 0.867), demonstrated robust clinical performance.

Conclusion: ME1, SLC2A1, and BMP4 are pivotal anoikis resistance-related biomarkers in COPD, driving immune dysregulation and structural remodeling. The developed models enable precise phenotyping, severity stratification, and personalized prognosis prediction, advancing precision medicine strategies for COPD management.

Keywords: anoikis resistance, COPD, emphysema, chronic bronchitis

Introduction

Chronic obstructive pulmonary disease (COPD) is a heterogeneous pulmonary disorder characterized by persistent respiratory symptoms (dyspnea, cough, and sputum production) resulting from chronic abnormalities of the airways (bronchitis, bronchiolitis), alveoli (emphysema), and/or pulmonary vasculature. It is defined by spirometrically confirmed airflow limitation and/or structural or physiologic pulmonary dysfunction.[1,2] COPD, currently ranked as the third leading cause of global mortality,[3,4] is projected to affect nearly 600 million individuals worldwide by 2050.[5] In China, this prevalent chronic respiratory condition affects 8.2% of adults[6,7] and has been incorporated into national chronic disease management programs alongside hypertension and diabetes. The main risk factors for COPD include smoking, biomass fuel exposure, and other environmental pollutants,[8] manifesting histologically as chronic bronchitis and emphysema.[9] Emerging evidence implicates several interconnected pathological mechanisms including chronic inflammation, oxidative stress, cellular senescence, and importantly, dysregulated apoptosis.[10,11] Of particular relevance, apoptosis/death of

https://doi.org/10.2147/JIR.S534626
Received: 15 April 2025
Accepted: 31 August 2025
Published: 6 September 2025

© 2025 Hu et al. This work is published and licensed by Dove Medical Press Limited. The full terms of this license are available at https://www.dovepress.com/terms.php and incorporate the Creative Commons Attribution – Non Commercial (unported, v4.0) License (http://creativecommons.org/licenses/by-nc/4.0/). By accessing the work you hereby accept the Terms. Non-commercial uses of the work are permitted without any further permission from Dove Medical Press Limited, provided the work is properly attributed. For permission for commercial use of this work, please see paragraphs 4.2 and 5 of our Terms (https://www.dovepress.com/terms.php).

cells is a key pathophysiological mechanism leading to airway epithelial damage/repair and emphysema formation in COPD patients. However, the precise contribution of apoptotic pathways to COPD phenotypic heterogeneity remains poorly characterized, particularly regarding their role in disease progression and phenotypic transitions.

Anoikis, a caspase-dependent form of programmed cell death, occurs upon disruption of cell-extracellular matrix (ECM) interactions.[12] This process is regulated through multiple signaling pathways involving RhoA, p66shc, and other cytoskeletal/adhesion proteins, culminating in apoptotic cell death.[13–16] Conversely, anoikis resistance, which has been extensively documented in various pathological conditions including malignant tumors, promotes tumor metastasis and progression by facilitating anchorage-independent growth (AIG).[17–19] Emerging evidence suggests that molecular pathways and mechanisms regulating anoikis resistance, including cell adhesion molecules, growth factors, and signaling pathways inducing epithelial-mesenchymal transition (EMT), also play important roles in COPD.[20–22] Nevertheless, the expression profiles and functional roles of anoikis resistance signaling in the pathogenesis and progression of COPD remain to be fully elucidated, warranting further investigation.

In this study, we employed LASSO regression and multiple machine learning algorithms to identify five core hub genes associated with anoikis resistance and validated their expression in COPD using population, animal, and cellular models. Subsequent clinical investigations revealed significant correlations between core hub genes expression (ME1, SLC2A1, and BMP4) and quantitative CT parameters of airway remodeling and emphysema severity. Ultimately, we optimized a COPD diagnostic and prognostic evaluation models, providing a foundation for the comprehensive prevention and treatment of COPD.

Materials and Methods

Differential Expression and Functional Enrichment Analysis of Anoikis Resistance-Related Genes

Expression profiles from the GSE11906 and GSE19407 datasets were downloaded from the Gene Expression Omnibus (GEO) database (https://www.ncbi.nlm.nih.gov/geo/). The GSE11906 dataset comprises 72 healthy individuals and 33 COPD patients, while the GSE19407 dataset included 47 healthy individuals and 22 COPD patients. All samples were obtained from the small airway epithelium via fiberoptic bronchoscopy. Anoikis resistance-related genes were obtained from GeneCards (https://www.genecards.org/), and differential gene expression analysis was performed using the "limma" R package (adj. $P < 0.05$, $|\log2FC| > 0.585$). Functional enrichment analysis of anoikis resistance-associated DEGs was performed using Gene Ontology (GO) and Kyoto Encyclopedia of Genes and Genomes (KEGG) pathway databases via the "clusterProfiler" R package. Adj. $P < 0.05$ was considered to be statistically significant in the enrichment results. Enrichment outcomes were visualized using the "ggplot2" R package. The "c2.cp.kegg.symbols.gmt" gene set was obtained from the MSigDB database, and Gene Set Enrichment Analysis (GSEA) was performed using the "ClusterProfiler" R package. $P < 0.05$, $|NES| > 1$, and FDR < 0.25 were considered to be statistically significant.

Identification of Core Hub Genes and Construction of the ceRNA Network

The "glmnet" R package was used for 10-fold cross-validation in LASSO regression analysis. Machine learning models, including random forest (RF), support vector machine (SVM), XGBoost (XGB), and generalized linear model (GLM), were constructed using the "caret", "DALEX", "ggplot2", "randomForest", "kernlab", "xgboost", and "pROC" R packages. Core hub genes associated with anoikis resistance were identified using the "VennDiagram" R package. Potential miRNA targets of the core hub genes were predicted using miRanda, miRDB, and TargetScan, while interactions between miRNAs and lncRNAs were predicted using the SpongeScan database. The lncRNA-miRNA-mRNA regulatory network was constructed and visualized using Cytoscape software (version 3.9.1).

Cell Culture and Cigarette Smoke Extract (CSE) Treatment

16HBE cells were purchased from Procell Life Science and Technology Co., Ltd (Wuhan, China) and cultured in MEM medium supplemented with 10% fetal bovine serum (FBS), penicillin (100 U/mL), and streptomycin (100 U/mL). CSE

was prepared as previously described by our research group,[23] and used to stimulate cells at concentrations of 3% and 5% for 24 hours prior to qRT-PCR detection. Each cell experiment was performed in triplicate.

RNA Extraction and Quantitative Real-Time PCR (qRT-PCR)

Total RNA was extracted using TRIzol reagent (Takara, 9108, Japan) following the manufacturer's instructions. cDNA synthesis was performed using a reverse transcription kit, and the transcription levels of UCHL1, ME1, SLC2A1, BMP4, and CRABP2 were detected using the SYBR Green PCR kit (Accurate Biology, AG11701, China). GAPDH served as the internal reference gene, and relative expression levels were calculated using the $2^{-\Delta\Delta CT}$ method. Primer sequences are provided in Table 1.

Table 1 Primer Sequences of the Panel Genes

Gene	Species	Primer Sequence (5′ to 3′)
UCHL1	Human	Forward: AACCCCGAGATGCTGAACAAAGTG
		Reverse: CACCGAGCCCAGAGACTCCTC
ME1	Human	Forward: GCTTGGGAGACCTTGGCTGTAATG
		Reverse: CCACATCCAGAATGACAGGCAGAC
SLC2A1	Human	Forward: TTGGCCGGCGGAATTCAATG
		Reverse: TCAAAGGACTTGCCCAGTTTCG
BMP4	Human	Forward: GCGATGTGGGCTGGAATGACTG
		Reverse: ATGGCATGGTTGGTTGAGTTGAGG
CRABP2	Human	Forward: GCCCTGTAAGAGCCTGGTGAAATG
		Reverse: AGTTCTCTGGTCCACGAGGTCTTG
GAPDH	Human	Forward: CAACGTGTCAGTGGTGGACCTG
		Reverse: GTGTCGCTGTTGAAGTCAGAGGAG
UCHL1	Mouse	Forward: AACCCCGAGATGCTGAACAAAGTG
		Reverse: AGAGTCTCCTCCTCCAGCCCTAG
ME1	Mouse	Forward: GTGAACCCACAACAGTGTCTACCC
		Reverse: TCCAGGAAGGCGTCATACTCAGG
SLC2A1	Mouse	Forward: GTGCTCCTCGTGCTCTTCTTCATC
		Reverse: CTCCTCGGGTGTCTTGTCACTTTG
BMP4	Mouse	Forward: GCCAACACTGTGAGGAGTTTCC
		Reverse: TTCTCTGGGATGCTGCTGAGG
CRABP2	Mouse	Forward: AGCCTCCAAGCCAGCAGTCG
		Reverse: TTAATCTCCGTGGTTCGCACAGTG
GAPDH	Mouse	Forward: CATCACTGCCACCCAGAAGACTG
		Reverse: ATGCCAGTGAGCTTCCCGTTCAG

https://doi.org/10.2147/JIR.S534626

Construction of CSE-Induced COPD Mouse Model

Twelve 8-week-old male C57BL/6 mice were procured from Jinan Pengyue Experimental Animal Breeding Co., Ltd. (Jinan, China) and randomly assigned to two experimental cohorts (n = 6 per group): an age-matched control group and a chronic cigarette smoke-induced COPD model group. Mice in the smoke exposure group were placed in a passive cigarette smoke exposure twice daily, with seven Tai Shan brand cigarettes (tar 11 mg/cigarette, nicotine 1.1 mg/cigarette, and carbon monoxide 11 mg/cigarette) burned per session, for 2 hours each time (maintaining CO_2 concentration at 800–1300 ppm and O_2 concentration above 18% during exposure), for 24 weeks.

Assessment of Lung Function in Animals

Lung function parameters, including peak expiratory flow (PEF), maximum mid-expiratory flow (MMEF), and the ratio of forced expiratory volume at 25ms, 50ms, 75ms, and 100ms to forced vital capacity (FEV25ms/FVC, FEV50ms/FVC, FEV75ms/FVC, FEV100ms/FVC), were measured using the EMMS Forced Maneuvers system (EMMS-CRFM100, EMMS, UK).

Pulmonary Histopathology

The isolated left lung tissues from mice were subjected to qRT-PCR analysis described in Section qRT-PCR. The right lung tissues were fixed in 4% paraformaldehyde, embedded in paraffin, and sectioned. Tissue sections were stained with hematoxylin (Solarbio, H8070, Beijing, China) and eosin (Sangon, A600190, Shanghai, China) for histological evaluation. Images were captured using an inverted microscope for subsequent morphological analysis. Mean linear intercept (MLI): MLI = L/Ns (reflecting the average alveolar diameter) and mean alveolar number (MAN): MAN = Na/S (reflecting alveolar density).

Immunohistochemistry (IHC)

5 μm sections of paraffin-embedded tissues were dewaxed, rehydrated, and subjected to antigen retrieval with citrate buffer (pH 6.0). After blocking with 10% goat serum, the sections were incubated overnight at 4°C with an anti-α-SMA antibody (80008-1-RR, Proteintech). Subsequently, the sections were incubated with an HRP-conjugated secondary antibody, stained with 3,3′-diaminobenzidine (DAB) and counterstained with hematoxylin.

Human Sample Collection

From September to December 2024, 50 patients with COPD (44 males, 6 females; aged 40–85 years) were recruited from the Department of Respiratory and Critical Care Medicine, Qingdao Municipal Hospital, along with 40 age-matched healthy controls from the health check-up center. All participants underwent spirometry at enrollment, with 35 also undergoing high-resolution computed tomography (HRCT). The constructed models were randomly partitioned into training and internal validation sets at a 7:3 ratio. According to the Global Initiative for Chronic Obstructive Lung Disease (GOLD, 2025) guidelines, COPD severity was classified into early-stage (GOLD 1–2) and late-stage (GOLD 3–4) patients. Patient prognosis was stratified based on the median length of hospitalization.

Univariate analysis indicated no statistically significant differences in baseline characteristics between all the training and validation cohorts, including age, gender, pulmonary function parameters, emphysema severity (quantified by LAA %), airway remodeling (assessed via the square root of airway wall area at an internal perimeter of 10 mm, AWT-Pi10), and hospitalization duration (all $P > 0.05$; detailed in Tables 2–4). The study was approved by the Medical Ethics Committee of Qingdao Municipal Hospital, and written informed consent was obtained from all participants (2025-KY-105).

Isolation of Peripheral Blood Mononuclear Cells (PBMCs)

Following informed consent, whole blood samples were collected from all enrolled participants. PBMCs were isolated using Ficoll density gradient centrifugation according to the manufacturer's protocol (Solarbio, Beijing, China). Briefly, blood samples were centrifuged at 2000 rpm for 10 minutes at 4°C. After centrifugation, the serum and red blood cell layer were carefully removed, and the intermediate leukocyte layer was collected. The PBMCs were washed twice with

Table 2 The Baseline Characteristics of Validation and Training Cohorts for the Emphysema Pathological Phenotype Diagnostic Model

Variables	Total (n = 35)	Validation Cohort (n = 11)	Training Cohort (n = 24)	*P*
Gender, n (%)				
Male	31 (88.57)	10 (90.91)	21 (87.50)	1.000
Female	4 (11.43)	1 (9.09)	3 (12.50)	
Age (years, mean ±SD)	68.00 ± 8.29	67.36 ± 8.13	68.29 ± 8.51	0.763
FVEV1, %, mean ± SD	51.38 ± 15.31	56.39 ± 12.72	49.00 ± 16.13	0.214
FVC, %, mean ± SD	69.75 ± 20.23	66.95 ± 24.47	71.09 ± 18.41	0.603
FEV1/FVC, %, mean ± SD	62.99 ± 13.86	67.89 ± 12.63	60.66 ± 14.09	0.179
AWT-Pi10, mm, mean ± SD	4.57 ± 0.57	4.63 ± 0.43	4.54 ± 0.63	0.687
LAA, %, Median (IQR)	0.09 (0.01, 0.23)	0.14 (0.03, 0.25)	0.08 (0.01, 0.17)	0.486
Length of stay, (days, mean ± SD)	8.29 ± 1.93	8.00 ± 2.10	8.42 ± 1.89	0.562

Table 3 The Baseline Characteristics of Validation and Training Cohorts for the Early/Late-Stage COPD Diagnostic Model

Variables	Total (n = 50)	Validation Cohort (n = 15)	Training Cohort (n = 35)	*P*
Gender, n (%)				
Male	44 (88.00)	13 (86.67)	31 (88.57)	1.000
Female	6 (12.00)	2 (13.33)	4 (11.43)	
Age (years, mean ±SD)	66.90 ± 7.71	66.40 ± 6.91	67.11 ± 8.12	0.768
FVEV1, %, mean ± SD	50.96 ± 16.77	53.97 ± 17.04	49.77 ± 16.77	0.450
FVC, %, Median (IQR)	67.25 (50.35, 77.97)	60.30 (47.60, 75.80)	70.80 (51.10, 78.00)	0.510
FEV1/FVC, %, mean ± SD	60.62 ± 15.22	60.28 ± 13.62	60.76 ± 16.01	0.926
AWT-Pi10, mm, Median (IQR)	4.50 (4.20, 4.85)	4.70 (4.40, 4.90)	4.50 (4.10, 4.70)	0.256
LAA, %, mean ± SD	0.14 ± 0.15	0.14 ± 0.14	0.13 ± 0.15	0.832
Length of stay, (days, mean ± SD)	8.10 ± 2.12	8.00 ± 2.88	8.14 ± 1.75	0.830

Table 4 The Baseline Characteristics of Validation and Training Cohorts for the Hospital Stay Duration Prognostic Model

Variables	Total (n = 50)	Validation Cohort (n = 15)	Training Cohort (n = 35)	*P*
Gender, n (%)				
Male	44 (88.00)	14 (93.33)	30 (85.71)	0.776
Female	6 (12.00)	1 (6.67)	5 (14.29)	
Age (years, mean ±SD)	66.90 ± 7.71	67.20 ± 7.36	66.77 ± 7.96	0.859
FVEV1, %, mean ± SD	53.08 ± 20.53	57.65 ± 26.09	51.46 ± 18.38	0.376
FVC, %, mean ± SD	62.61 ± 29.62	70.30 ± 27.82	59.90 ± 30.16	0.301
FEV1/FVC, %, mean ± SD	61.23 ± 16.86	64.96 ± 18.55	59.92 ± 16.31	0.380
AWT-Pi10, mm, Median (IQR)	4.55 ± 0.57	4.47 ± 0.40	4.60 ± 0.64	0.519
LAA, %, mean ± SD	0.14 ± 0.15	0.17 ± 0.18	0.12 ± 0.12	0.286
Length of stay, (days, Median (IQR))	8.00 (6.25, 9.00)	8.00 (6.00, 8.50)	8.00 (7.00, 9.00)	0.390

phosphate-buffered saline (PBS), centrifuged at 1500 rpm for 10 minutes each time, and the cell pellets were stored at −80°C for subsequent analysis. The transcriptional levels of UCHL1, ME1, SLC2A1, BMP4, and CRABP2 in PBMCs were determined by qRT-PCR following the protocol described in Section qRT-PCR.

Quantitative Analysis of HRCT Images

HRCT images of COPD patients were obtained using the Picture Archiving and Communication System (PACS), and the original DICOM format images were loaded into the A-View® artificial intelligence lung quantitative imaging software (Suzhou Suhai Information Technology Co., Ltd., China) for automatic quantitative analysis to obtain the LAA% and AWT-Pi10. Subsequently, COPD patients were categorized into non-emphysema (COPD-NE, LAA% < 6%) and emphysema (COPD-E, LAA% ≥ 6%) groups based on LAA% levels.

Statistical Analysis

Statistical analyses were performed using R software (version 4.4.1), SPSS 26.0 software and GraphPad Prism 9 software. The Shapiro–Wilk test was used to assess data normality. Continuous variables are presented as median (interquartile range) or mean ± standard deviation (mean ± SD). Comparisons between two groups were made using independent sample *t*-test or Mann–Whitney *U*-test. Categorical variables are presented as numbers (%), and comparisons between two groups were performed using the χ^2 test or Fisher's exact test. ANOVA was used for multi-group comparisons, and Spearman and Pearson tests were used for correlation analyses. The performance of diagnostic and prognostic models was assessed using the area under the receiver operating characteristic curve (AUC-ROC). Calibration curves were utilized to evaluate model calibration, while decision curve analysis (DCA) was performed to determine clinical utility. $P < 0.05$ (two-sided) was considered statistically significant.

Results

Screening and Functional Enrichment Analysis of Differentially Expressed Anoikis Resistance Genes

To investigate the potential genes of anoikis resistance in COPD pathogenesis, we obtained 913 anoikis resistance-related genes from GeneCards and extracted their expression profiles from the GSE11906 dataset. A total of 75 DEGs were identified, comprising 39 upregulated and 36 downregulated genes (|log FC| > 0.586, adj. $P < 0.05$, Figure 1A and B).

To further reveal the potential functions of these DEGs in COPD, GO and KEGG pathway enrichment analyses were performed. The results showed that these DEGs were significantly associated with 1365 GO terms and 65 KEGG pathways. The top 30 GO terms and KEGG pathways are shown in Figure 1C and D. GO enrichment analysis indicated that, in the biological process (BP) domain, these genes were mainly involved in "regulation of epithelial cell proliferation" and "positive regulation of cell adhesion". In the cellular component (CC) domain, they were primarily associated with "collagen-containing extracellular matrix" and "focal adhesion". In the molecular function (MF) domain, they were mainly linked to "DNA-binding transcription factor binding" and "cytokine activity". KEGG pathway analysis indicated that anoikis resistance-related DEGs were mainly enriched in pathways such as "PI3K-Akt signaling pathway", "MAPK signaling pathway" and "Cytokine-cytokine receptor interaction".

Identification and External Dataset Validation of Core Hub Genes of Anoikis Resistance

To identify core hub genes related to COPD, we analyzed the 75 DEGs using LASSO Cox regression and four machine learning algorithms (RF, SVM, XGB, and GLM). In the LASSO regression analysis, 10-fold cross-validation identified 20 key genes (Figure 2A and B). Subsequently, based on the RF, SVM, XGB, and GLM machine learning models, the top 10 most important genes were selected by each algorithm. After comparing the predictive performance of the models, the RF model demonstrated superior performance and was selected for further analysis (Figure 2C–E). By intersecting the key genes selected by LASSO regression and the RF model, five core hub genes were ultimately identified (Figure 2F), including UCHL1, ME1, SLC2A1, BMP4, and CRABP2. Compared to the healthy control group, the expression levels of UCHL1, ME1, SLC2A1, and BMP4 was significantly upregulated in the COPD group, while the expression of CRABP2 was significantly downregulated.

To further validate the expression patterns of these genes, we analyzed the external dataset GSE19407. The results showed that, except for CRABP2 ($P = 0.057$), the expression of UCHL1 ($P = 2.3e\text{-}15$), ME1 ($P = 2.22e\text{-}16$), SLC2A1

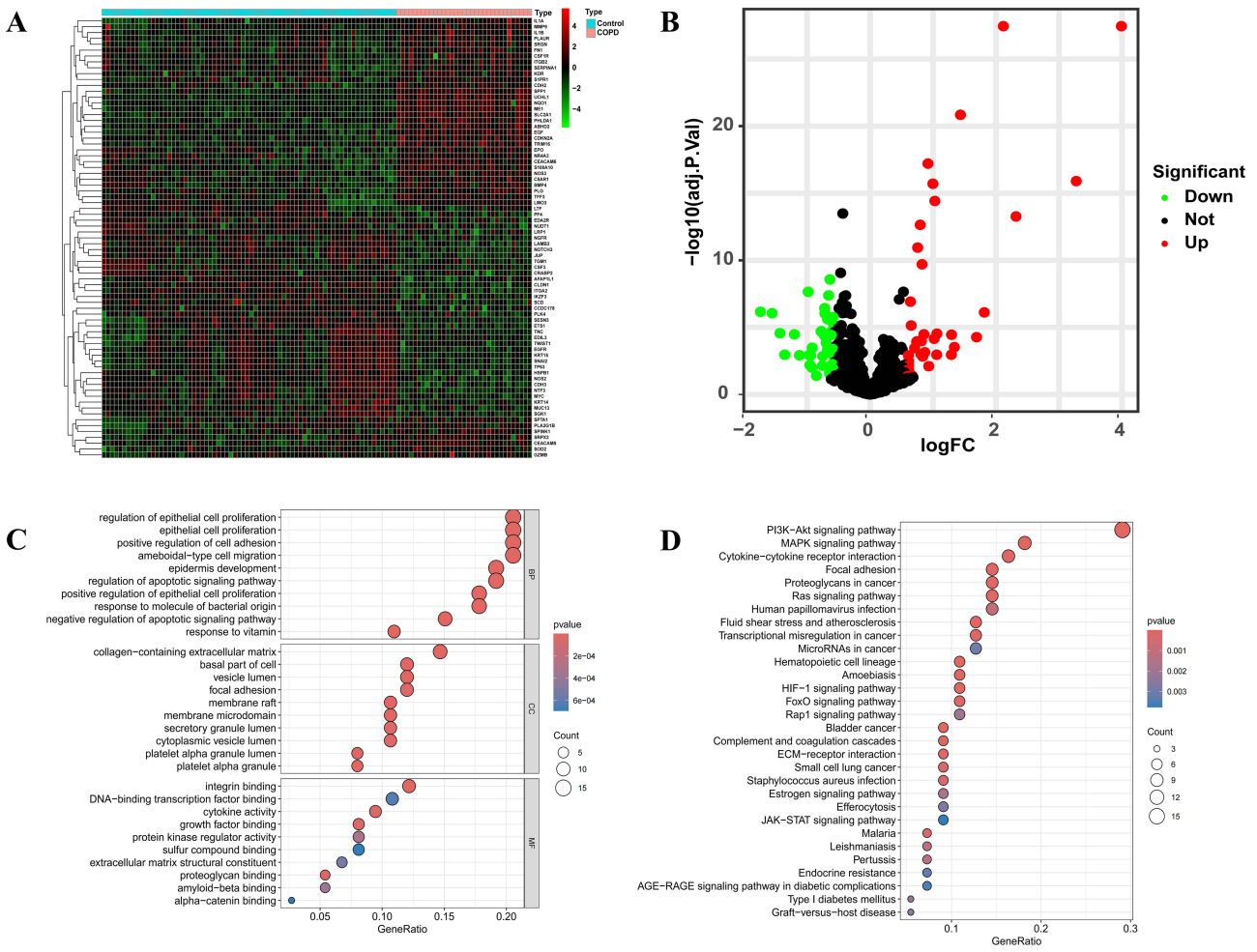

Figure 1 Expression patterns of DEGs in COPD. (**A**) Heatmap of DEG expression. (**B**) Volcano plot of DEGs. (**C**) GO enrichment analysis. (**D**) KEGG pathway analysis.

(P = 1.2e-12), and BMP4 (P = 0.023) was significantly higher in the COPD group compared to the control group (Figure S1).

GSEA Reveals Potential Mechanisms of Core Hub Genes in COPD Regulation

To further elucidate the biological functions of UCHL1, ME1, SLC2A1, BMP4, and CRABP2 in COPD, we performed GSEA-KEGG pathway enrichment analysis, showing the top six pathways enriched for each core hub gene (Figure S2). GSEA results revealed that these genes were significantly involved in pathways such as "NATURAL_KILLER_CELL_MEDIATED_CYTOTOXICITY", "CYTOKINE_CYTOKINE_RECEPTOR_INTERACTION", "REGULATION_OF_AUTOPHAGY" and various metabolic pathways. These findings suggest that the core hub genes may play critical roles in COPD pathogenesis by modulating immune responses or cellular metabolic processes.

Correlation of Core Hub Genes with Immune Cell Infiltration

The GSEA results suggested that these five core hub genes might be involved in immune regulation in COPD. To further validate this hypothesis, we employed the CIBERSORT algorithm to analyze differences in peribronchial immune cell infiltration between COPD patients and healthy controls, presenting the distribution of immune cell proportions as a stacked histogram (Figure 3A). Violin plot results that the infiltration proportions of plasma cells, T cells CD8, T cells

https://doi.org/10.2147/JIR.S534626

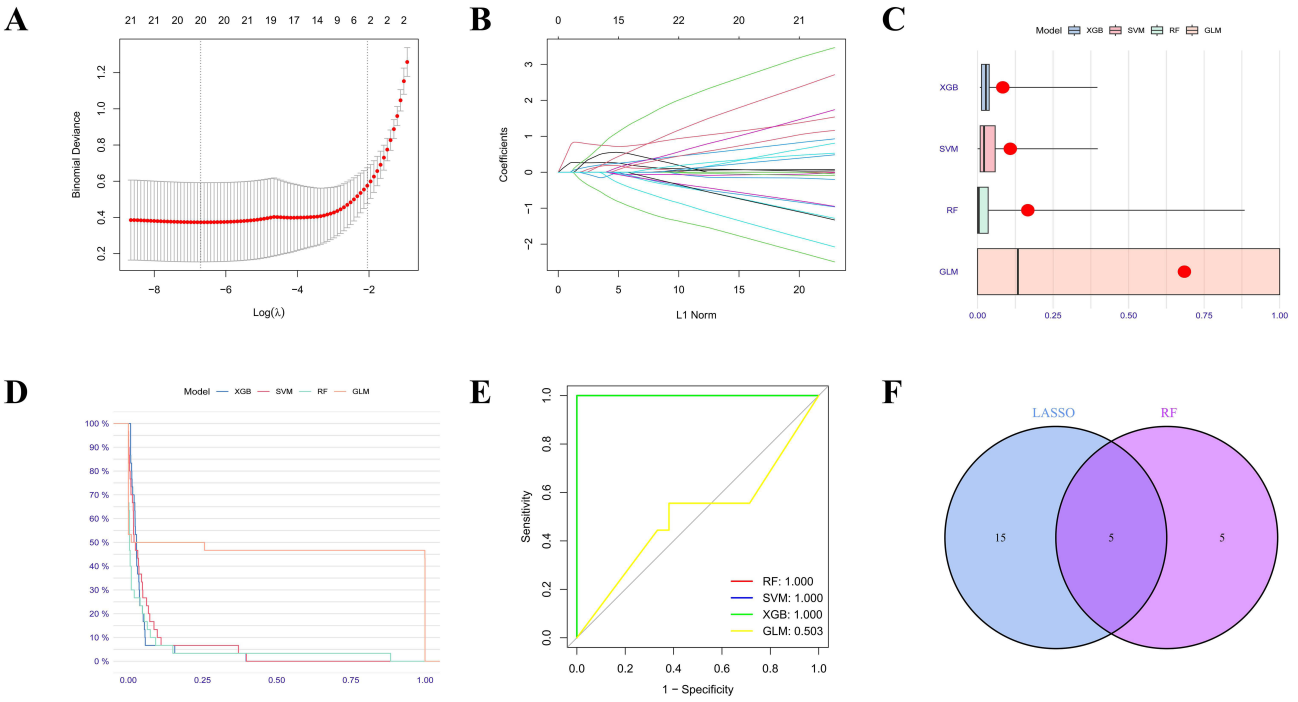

Figure 2 Identification of core anoikis resistance genes. (**A-B**) LASSO algorithm. Using the LASSO algorithm, we identified 20 feature genes in COPD. (**C**) Boxplot showing sample residuals, with red dots representing the root mean square of residuals. (**D**) Reverse cumulative distribution of residuals in four machine learning models. (**E**) ROC evaluation of the performance of RF, SVM, XGB, and GLM models. (**F**) Intersection of key genes selected by LASSO and RF algorithms to identify five core hub genes.

follicular helper, macrophages M0, and macrophages M1 were significantly higher in the COPD group (Figure 3B), indicating that these immune cells might play key roles in COPD progression.

Furthermore, we investigated the correlation between the expression of core hub genes and peribronchial immune cell infiltration within the COPD group. The associations between UCHL1, ME1, SLC2A1, BMP4, and CRABP2 expression and various immune cell subsets were visualized using lollipop plots (Figure 3C–G). The results revealed that the expression of these genes was significantly correlated with the infiltration of immune cells such as T cells CD8 and T cells follicular helper. Collectively, these findings suggest that the five core hub genes may play essential roles in immune regulation in COPD, providing a foundation for further exploration of the potential mechanisms of anoikis resistance in this disease.

Construction of the ceRNA Network

Recent studies have highlighted the regulatory roles of long non-coding RNAs (lncRNAs) and microRNAs (miRNAs) in disease progression by modulating mRNA expression.[24,25] To investigate the investigate upstream miRNAs and lncRNAs regulating the five core hub genes, we constructed a ceRNA network, revealing intricate interactions among lncRNAs, miRNAs, and core hub genes. As illustrated in Figure 3H, the network comprises five core hub genes, 122 miRNAs, and 180 lncRNAs. These results demonstrate that anoikis resistance is closely associated with these lncRNAs and miRNAs, thereby influencing COPD disease progression.

Expression of Core Hub Genes in Cell Models

To validate the expression patterns of the core hub genes in COPD, we performed qRT-PCR to assess the expression levels of the five core hub genes in 16HBE cells stimulated with varying concentrations of CSE. The results revealed that, compared with the control group, the expression of ME1, SLC2A1, and BMP4 was significantly upregulated in the CSE-stimulated groups (Figure 4A–E). Notably, in contrast to the dataset results, CRABP2 exhibited a divergent expression trend in the CSE-stimulated groups compared to the control, suggesting that its regulatory mechanisms may be more complex.

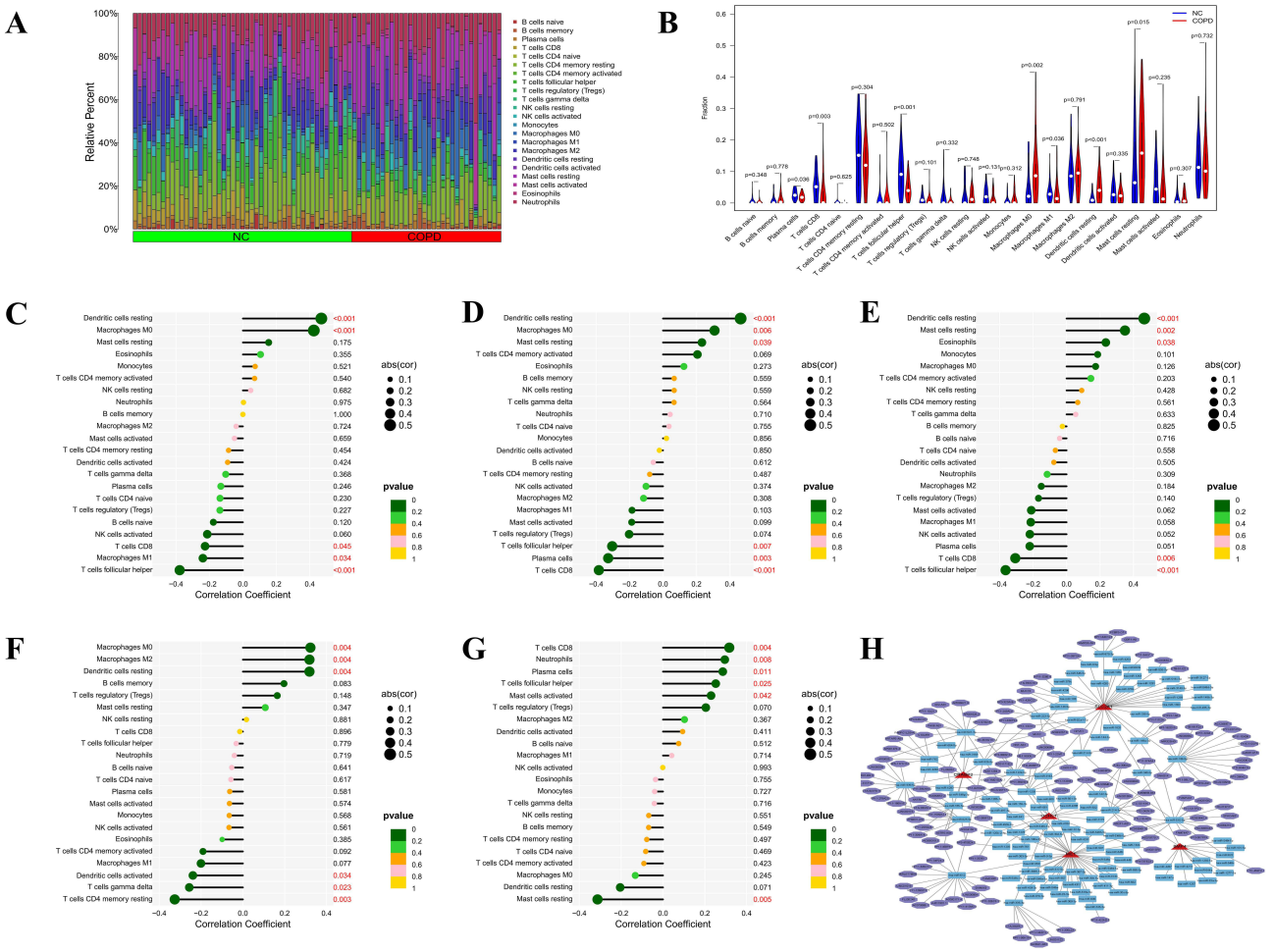

Figure 3 Immune infiltration results from CIBERSORT and ceRNA network. (**A**) The CIBERSORT algorithm was used to map 22 kinds of immune cells in t COPD patients and healthy cohorts of GSE11906 dataset. (**B**) The immune cell infiltration between between COPD patients and healthy cohorts of GSE11906 dataset. (**C**) The association between UCHL1 and different immune cell infiltration in COPD. (**D**) The association between ME1 and different immune cell infiltration in COPD. (**E**) The association between SLC2A1 and different immune cell infiltration in COPD. (**F**) The association between BMP4 and different immune cell infiltration in COPD. (**G**) The association between CRABP2 and different immune cell infiltration in COPD. (**H**) ceRNA network of UCHL1, ME1, SLC2A1, BMP4, and CRABP2. Red represents mRNA, blue represents miRNA, and purple represents lncRNA. **P* < 0.05, ***P* < 0.01, ****P* < 0.001.

Expression of Core Hub Genes in COPD Mouse Models

COPD mouse model was successfully established through cigarette smoke exposure. Compared with the control group, the smoke-exposed group exhibited significant deterioration in pulmonary function parameters. Histopathological examination of lung tissues revealed characteristic features of emphysema and airway remodeling in the smoke-exposed group (Figure 5). Further qRT-PCR analysis of core hub genes expression in mouse lung tissues showed that the expression of UCHL1, ME1, SLC2A1, and BMP4 was significantly upregulated in the COPD mouse model, while the expression of CRABP2 showed a downward trend, although the difference was not statistically significant (Figure 4F–J).

Expression of Core Hub Genes in PBMCs of COPD Patients

Total RNA was extracted from PBMCs of COPD patients and healthy controls in the modeling group and detected the transcriptional levels of core hub genes using qRT-PCR. The results showed that, compared with the healthy control group, the expression of UCHL1, ME1, SLC2A1, and BMP4 was significantly upregulated in COPD patients, while the expression of CRABP2 was markedly downregulated (Figure 4K–O).

https://doi.org/10.2147/JIR.S534626

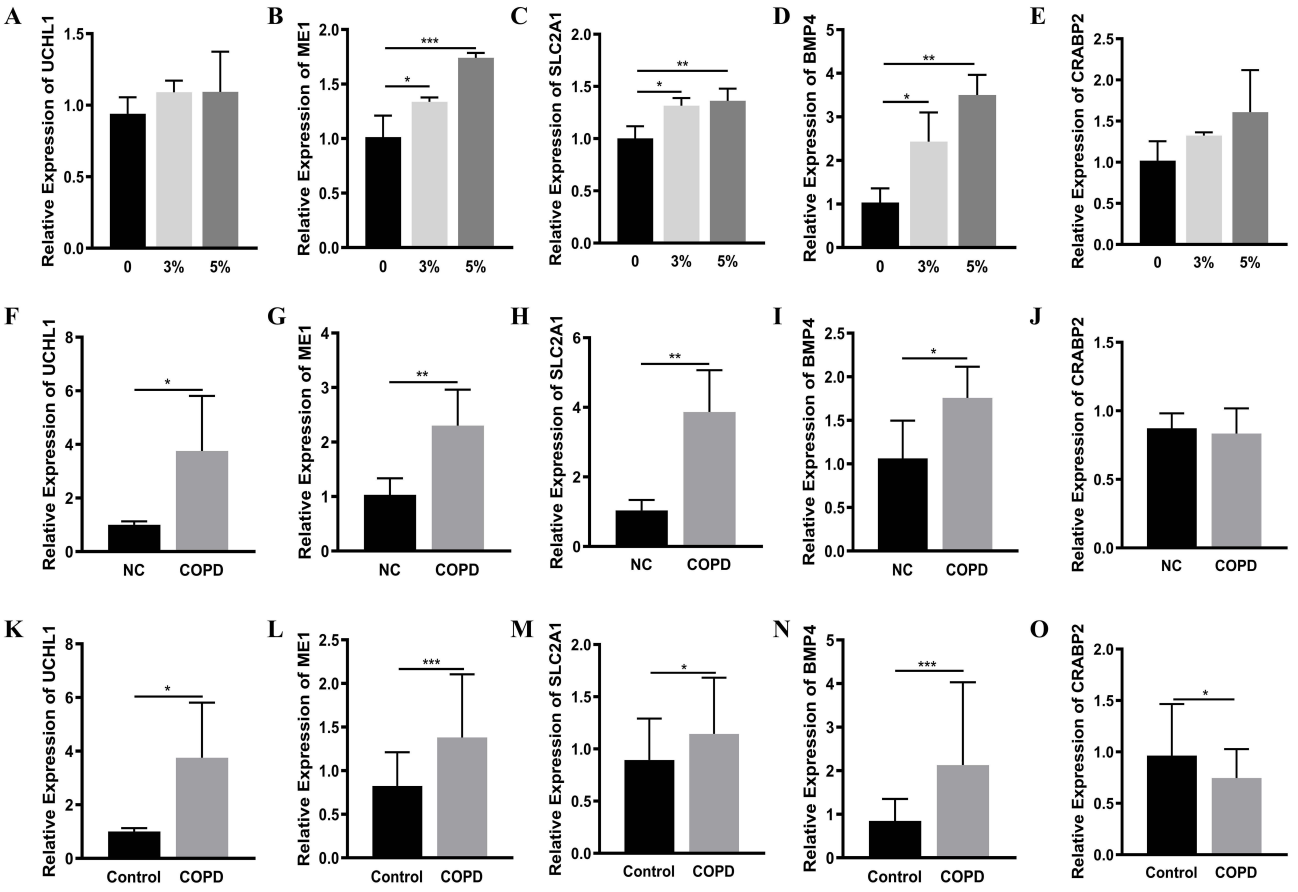

Figure 4 Validation of core hub gene expression in COPD cell and animal models, as well as in Clinical COPD Patient PBMCs by qRT-PCR. (**A-E**) Expression levels of the five core hub genes in 16HBE cells stimulated with different concentrations of CSE. (**F-J**) Expression levels of the five core hub genes in mouse lung tissues. (**K-O**) Expression levels of the five core hub genes in PBMCs of clinical COPD patients. Data are presented as mean ± SD. **P* < 0.05, ***P* < 0.01, ****P* < 0.001.

Application of Core Hub Genes in COPD Clinical Diagnostic Models

Given the consistent and significant differential expression of ME1, SLC2A1, and BMP4 across all experimental results, we further evaluated their potential value in COPD diagnosis and prognosis assessment. Correlation analyses revealed that their expression levels were significantly negatively associated with LAA%, while showing positive correlations with AWT-Pi10 (Figure 6). These findings strongly implicate their potential involvement in the pathological processes of emphysema progression and airway remodeling in COPD. We subsequently developed two robust diagnostic models using binary logistic regression: an emphysema phenotype diagnostic model: $P = \exp(-0.905 \times \text{ME1} - 3.657 \times \text{SLC2A1} - 0.284 \times \text{BMP4}) + 5.276$, and a disease severity staging model: $P = \exp(-0.63 \times \text{ME1} - 2.113 \times \text{SLC2A1} - 1.998 \times \text{BMP4}) + 5.112$, both demonstrating excellent calibration, as evidenced by close alignment with ideal calibration curves, and showed significant clinical net benefits across wide threshold probability ranges in DCA (Figure 7A and B).

The emphysema model showed particularly strong performance in the training cohort (AUC = 0.860, 95% CI: 0.705–1.000; sensitivity = 84.62%, specificity = 81.82%) that was maintained in validation (AUC = 0.714, 95% CI: 0.366–1.000; sensitivity = 100%, specificity = 50%). Similarly, the disease severity classification model showed outstanding training performance (AUC = 0.882, 95% CI: 0.775–0.990; sensitivity = 100.00%, specificity = 61.11%) and validation performance (AUC = 0.857, 95% CI: 0.643–1.000; sensitivity = 100%, specificity = 71.43%) (Figure 7A and B).

Application of Core Hub Genes in COPD Prognostic Evaluation Models

Building upon our established diagnostic models, we further evaluated their prognostic value by developing a hospitalization duration prediction model:$P = \exp(-0.694 \times \text{ME1} - 0.840 \times \text{SLC2A1} - 1.216 \times \text{BMP4}) + 4.473$.

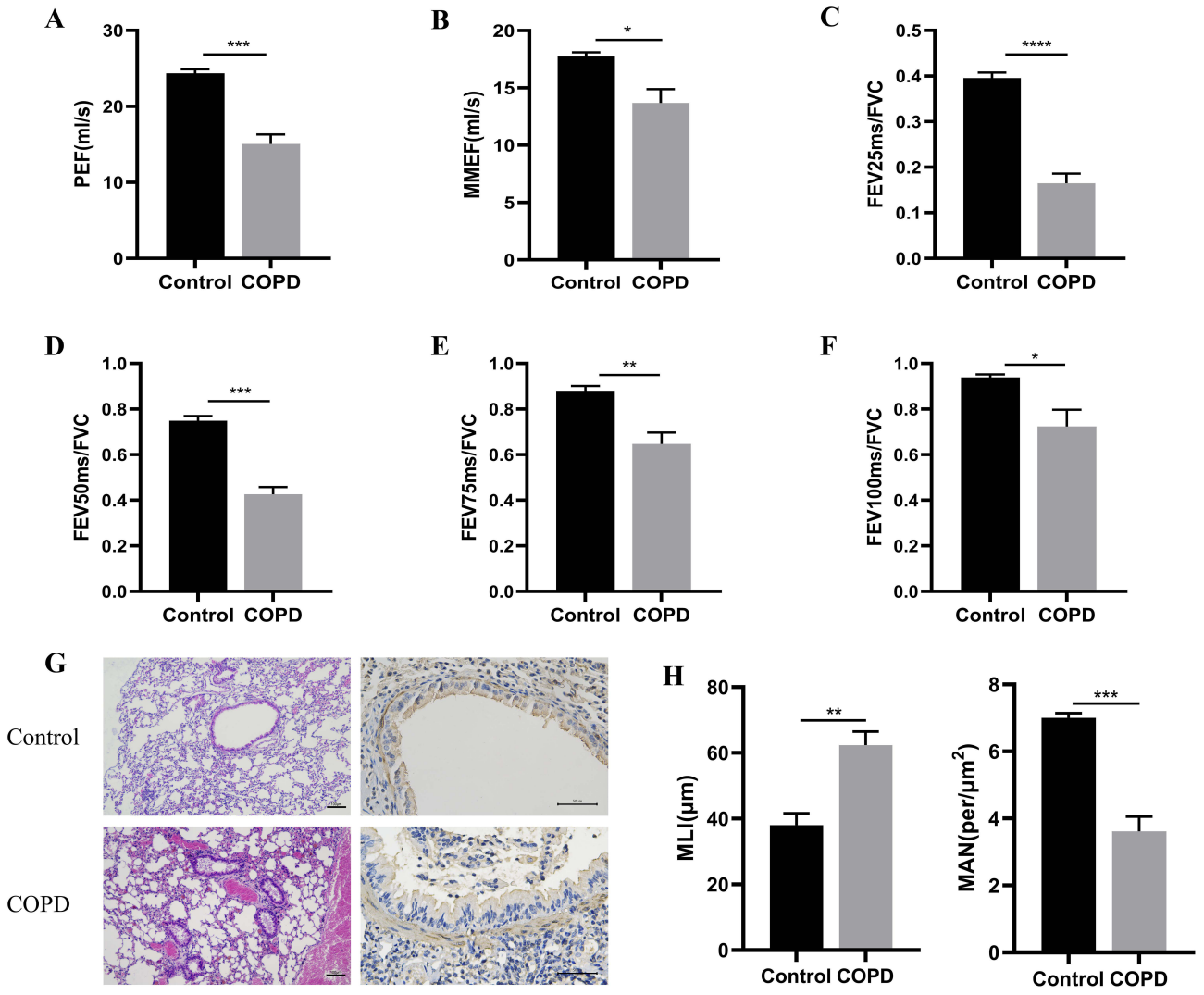

Figure 5 Pulmonary function parameters in mice were measured using the FM animal forced pulmonary function testing system. (**A**) PEF. (**B**) MMEF. (**C**) FEV25ms/FVC. (**D**) FEV50ms/FVC. (**E**) FEV75ms/FVC. (**F**) FEV100ms/FVC. (**G**) Representative images of H&E-stained lung tissue sections and IHC-stained sections for anti-human α-SMA (brown). (**H**) Mean linear intercepts (MLI) and mean alveolar number (MAN) in each group. *P < 0.05, **P < 0.01, ***P < 0.001, ****P < 0.0001.

The model demonstrated exceptional predictive accuracy through calibration analysis and significant clinical utility in decision curve analysis. Performance metrics remained consistent across cohorts, with the training cohort achieving AUC = 0.867 (sensitivity 95.2%, specificity 64.3%) and validation cohort showing AUC = 0.796 (sensitivity 88.9%, specificity 66.7%) (Figure 7C).

Collectively, our ME1/SLC2A1/BMP4-based models provide a comprehensive diagnostic-prognostic framework for COPD management, enabling: precise emphysema phenotyping, objective severity stratification, and individualized hospitalization risk prediction. These biomarkers show particular promise for guiding therapeutic decisions in clinical practice, potentially improving both diagnostic accuracy and patient outcomes through personalized medicine approaches.

Discussion

Chronic obstructive pulmonary disease (COPD) is a chronic inflammatory disorder characterized by heterogeneous pathological phenotypes such as chronic bronchitis and emphysema, for which endogenous biomarkers reflecting these pathological subtypes remain currently lacking. Through integrated bioinformatics analysis and systematic in vivo/in vitro validation, this study demonstrates elevated expression of anoikis resistance-associated core hub genes in COPD.

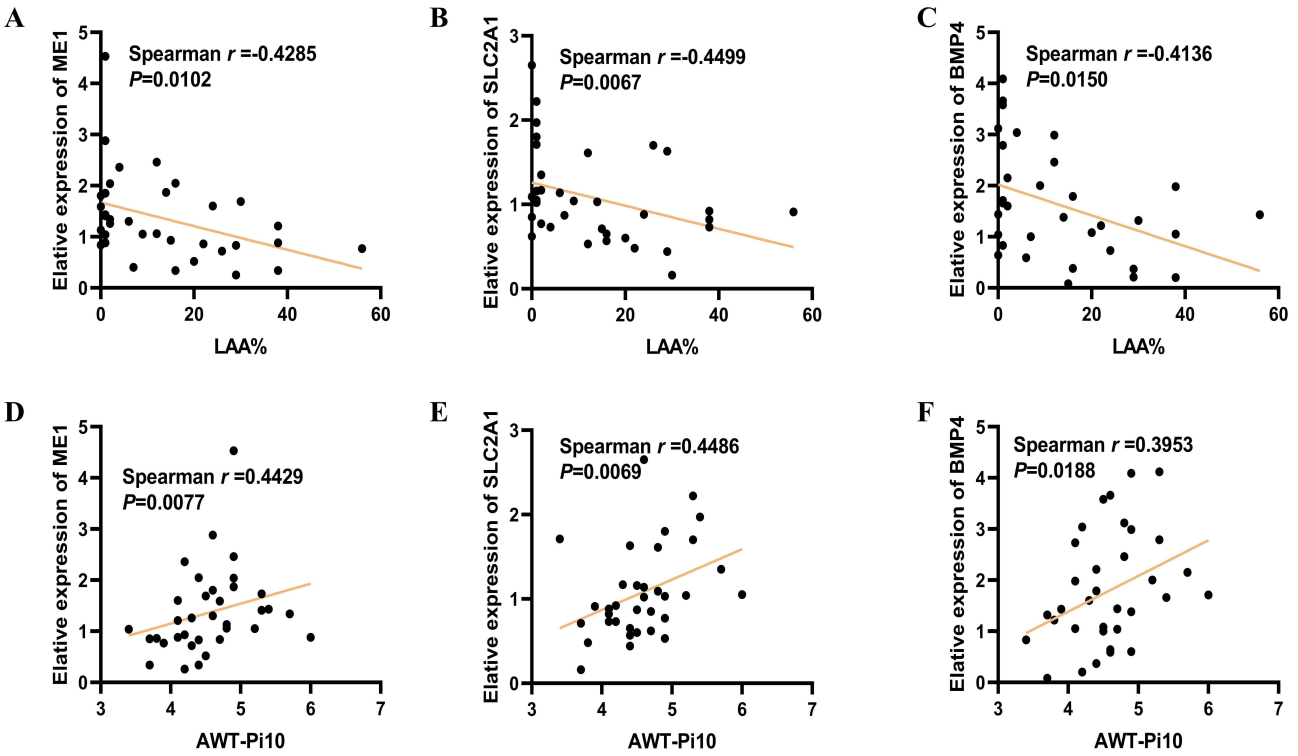

Figure 6 Correlation analysis of ME1, SLC2A1 and BMP4 expression with LAA% and AWT-Pi10 in COPD patients' PBMCs. (**A-C**) Correlation analysis of ME1, SLC2A1, and BMP4 with LAA%. (**D-F**) Correlation analysis with AWT-Pi10. *P < 0.05, **P < 0.01, ***P < 0.001.

We further reveal, for the first time, that the diagnostic and prognostic panels comprising core hub genes (ME1, SLC2A1, and BMP4) exhibits robust performance in distinguishing COPD phenotypes (chronic bronchitis and emphysema) and predicting disease severity, providing a novel biomarker panel for pathological subtyping and clinical assessment of COPD.

Recently, anoikis, a novel form of programmed cell death, has garnered considerable attention. Anoikis resistance, a pathophysiological phenomenon wherein cells survive despite detachment from the extracellular matrix (ECM), has been found to be aberrantly activated and closely associated with the development and progression of malignant tumors.[26,27] In COPD, abnormal proliferation/apoptosis is a critical pathogenic mechanism, with "emphysema" resulting from excessive alveolar epithelial apoptosis and "airway remodeling" arising from post-injury repair of the airway epithelium. However, the expression of anoikis resistance and its significance in disease evaluation in COPD remain unclear.

To elucidate the expression characteristics and underlying mechanisms of anoikis resistance-related signaling molecules in COPD, we conducted differential expression and functional enrichment analyses. These analyses revealed that anoikis resistance-related differentially expressed genes were significantly enriched in key signaling pathways closely associated with COPD pathogenesis, such as the PI3K-Akt and MAPK signaling pathways, as well as cytokine-cytokine receptor interactions (eg, inflammation, apoptosis, and oxidative stress). These findings suggest that anoikis resistance may contribute to COPD pathogenesis by modulating these biological processes.

Furthermore, CIBERSORT analyses revealed a markedly higher infiltration of M0 macrophages, M1 macrophages, and CD8 T cells in COPD tissues compared with healthy controls. These findings align with the CIBERSORT study by Feng Xu et al, which reported increased infiltration of CD4 T cells, CD8 T cells, and B lymphocytes in COPD specimens.[28] These findings not only validate the robustness of CIBERSORT in detecting immune microenvironment dysregulation, but also reveal macrophage polarization and T cell immunomodulation as pivotal directions for future mechanistic investigations in COPD.

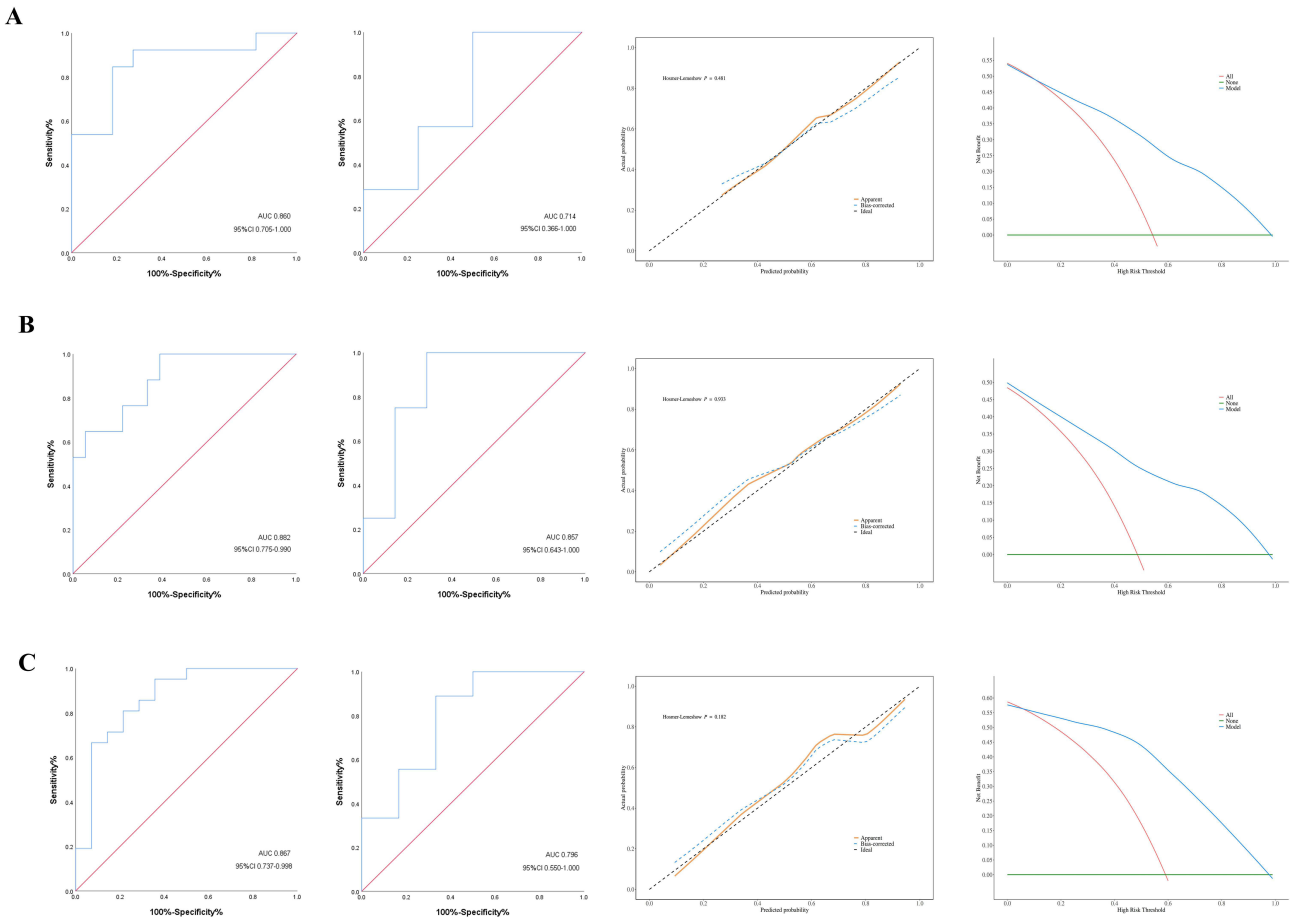

Figure 7 ROC curves, calibration plots, and DCA of the diagnostic and prognostic models. (**A**) Predictive performance of the three core hub genes for detecting emphysematous pathology in COPD patients, showing training cohort ROC, validation cohort ROC, calibration plot, and DCA. (**B**) Diagnostic performance in differentiating early- and late-stage COPD. (**C**) Predictive validity for hospitalization duration assessment.

Through LASSO regression and RF algorithm, we identified five core hub genes (UCHL1, ME1, SLC2A1, BMP4, and CRABP4) critically associated with anoikis resistance in COPD. Multi-level validation across COPD patient cohorts, animal and cellular models consistently demonstrated significant upregulation of ME1, SLC2A1, and BMP4 in both clinical specimens and experimental models. ME1 (malic enzyme 1), a key metabolic enzyme in the tricarboxylic acid (TCA) cycle, is closely linked to cellular proliferation.[29,30] Previous studies have demonstrated that ME1 is down-regulated in COPD-associated macrophages, where it modulates redox processes to influence mitochondrial ROS homeostasis and glycolytic balance, ultimately impairing macrophage effector functions.[31] Notably, the present study revealed elevated ME1 expression in lung tissues of COPD mice and PBMCs of patients, suggesting that it may have cell type-specific expression patterns and exert differentiated regulatory effects in distinct microenvironments. BMP4 (bone morphogenetic protein 4), a TGF-β superfamily member, not only participates in airway regeneration post-acute lung injury[32] but also promotes smoke-induced airway remodeling in COPD by driving aberrant differentiation of airway progenitor cells.[33] SLC2A1 (solute carrier family 2 member 1/GLUT1), a master regulator of glucose metabolism, contributes to disease progression through metabolic reprogramming, immune microenvironment remodeling, and anti-apoptotic mechanisms.[34–36] While its direct role in COPD remains undefined, emerging evidence implicates SLC2A1 in pulmonary pathologies: SLC2A1-dependent glycolysis exacerbates post-Streptococcus pneumoniae infection fibrosis via AIM2 inflammasome activation.[37] The TRPV4-SLC2A1 axis promotes phagolysosomal maturation through stiffness-dependent modulation of macrophage glycolysis to attenuate sepsis-induced lung injury.[38] Collectively, the dysregulated expression of these three hub genes implies their involvement in COPD pathogenesis through immunometabolic pathways, warranting further mechanistic investigation.

Based on the functional significance of anoikis resistance-related genes and their potential role in COPD pathogenesis, we further investigated the correlation between the expression of these core hub genes and COPD clinical phenotypes and pulmonary function severity. Our team previously utilized the A-View® platform and other artificial intelligence tools to characterize airway and vascular remodeling in populations occupationally exposed to diesel exhaust.[39,40] In this study, we employed A-View® software to analyze emphysema index (LAA%) and airway remodeling parameters (AWT-Pi10), revealing significant correlations between these core hub genes and CT imaging parameters, suggesting their potential as endogenous biomarkers for assessing COPD severity. Next, our study developed novel diagnostic models based on ME1, SLC2A1, and BMP4 expression profiles that effectively distinguished emphysematous subtypes (training AUC = 0.860; validation AUC = 0.714) and classified disease severity (training AUC = 0.882; validation AUC = 0.857 in COPD patients. Additionally, the prognostic model accurately predicted hospitalization duration (training AUC = 0.867; validation AUC = 0.796). These findings position the three-gene signature as a clinically valuable, noninvasive biomarker panel capable of facilitating personalized COPD management through comprehensive phenotypic characterization and risk assessment.

Additionally, numerous studies have highlighted that cytoplasmic lncRNAs can act as miRNA sponges, interfering with miRNA activity and thereby regulating mRNA stability or translation, ultimately influencing biological processes and contributing to various diseases.[41,42] Therefore, to explore potential upstream regulatory mechanisms of anoikis resistance, we constructed a ceRNA network centered on the core hub genes, revealing that they may be regulated by lncRNAs and miRNAs. This discovery provides new insights into the complex regulatory mechanisms of anoikis resistance in COPD.

While this study provides important insights into the role of anoikis resistance in COPD pathogenesis, several limitations should be considered when interpreting the findings. The relatively limited sample size, particularly within the validation cohort, constrains the statistical power of our findings. Future large-scale, multicenter studies are warranted to provide robust external validation of these results. Furthermore, the absence of validation across independent cohorts encompassing diverse geographic regions and ethnic populations represents a critical limitation for establishing generalizability. While our transcriptomic analysis identified key genes, integrating proteomic and metabolomic data would better characterize anoikis resistance in COPD. Most critically, the functional roles of hub genes (ME1/SLC2A1/BMP4) remain undefined, necessitating mechanistic studies using gene editing and functional assays to validate their pathophysiological contributions and therapeutic potential.

Conclusions

Anoikis resistance-related genes, represented by ME1, SLC2A1, and BMP4, are upregulated in COPD and are associated with peribronchial immune cell infiltration. We further establish, for the first time, their utility as clinically relevant biomarkers for emphysematous phenotype identification, objective disease severity stratification, and reliable prognosis prediction in COPD patients.

Data Sharing Statement

The datasets presented in this article can be found in online repositories. The names of the repositories and their accession numbers can be found in this article. The original data supporting the conclusions of this study have been provided by the authors without undue restrictions. These data can be found here: GeneCards (https://www.genecards.org/) and GEO database (https://www.ncbi.nlm.nih.gov/geo/) at accession numbers GSE11906 and GSE19407. Further inquiries can be addressed directly to the corresponding authors.

Ethics Approval and Consent to Participate

This animal experiment was approved by the Medical Ethics Committee of Qingdao Municipal Hospital. All the experiments were performed and analyzed in accordance with ARRIVE guidelines and guidelines for the ethical review of laboratory animal welfare (GB/T35892-2018) issued by China. The clinical samples were conducted according to the guidelines of the Declaration of Helsinki and approved by the Medical Ethics Committee of Qingdao Municipal Hospital (approval number: 2025-KY-105).

Acknowledgments

We thank all of our members for their valuable input and guidance.

Author Contributions

All authors made a significant contribution to the work reported, whether that is in the conception, study design, execution, acquisition of data, analysis and interpretation, or in all these areas; took part in drafting, revising or critically reviewing the article; gave final approval of the version to be published; have agreed on the journal to which the article has been submitted; and agree to be accountable for all aspects of the work.

Funding

This work was supported by grants from General Project of Shandong Provincial Natural Science Foundation, China (Grant No. ZR2024MH146): Study on the Role of Airway Epithelial MIF-Activated Macrophages in Diesel Exhaust-Induced Pulmonary Vascular Remodeling; and Qingdao Medical and Health Research Guidance Project (Grant No. 2024-WJKY016): Analysis of COPD Diagnosis and Treatment Status in Primary Medical Institutions and Construction of Disease Progression Prediction Models in Qingdao.

Disclosure

All authors report no conflicts of interest in this work.

References

1. Confalonieri M, Braga L, Salton F, Ruaro B, Confalonieri P. Chronic obstructive pulmonary disease definition: is it time to incorporate the concept of failure of lung regeneration? *Am J Respir Crit Care Med*. 2023;207(3):366–367. doi:10.1164/rccm.202208-1508LE
2. Celli B, Fabbri L, Criner G, et al. Definition and nomenclature of chronic obstructive pulmonary disease: time for its revision. *Am J Respir Crit Care Med*. 2022;206(11):1317–1325. doi:10.1164/rccm.202204-0671PP
3. Agusti A, Böhm M, Celli B, et al. GOLD COPD DOCUMENT 2023: a brief update for practicing cardiologists. *Clin Res Cardiol*. 2024;113(2):195–204. doi:10.1007/s00392-023-02217-0
4. Halpin DMG, Criner GJ, Papi A, et al. Global initiative for the diagnosis, management, and prevention of chronic obstructive lung disease. The 2020 GOLD science committee report on COVID-19 and chronic obstructive pulmonary disease. *Am J Respir Crit Care Med*. 2021;203(1):24–36. doi:10.1164/rccm.202009-3533SO
5. Boers E, Barrett M, Su JG, et al. Global burden of chronic obstructive pulmonary disease through 2050. *JAMA Network Open*. 2023;6(12):e2346598. doi:10.1001/jamanetworkopen.2023.46598
6. Fang L, Gao P, Bao H, et al. Chronic obstructive pulmonary disease in China: a nationwide prevalence study. *Lancet Respir Med*. 2018;6(6):421–430. doi:10.1016/s2213-2600(18)30103-6
7. Hu W, Fang L, Zhang H, Ni R, Pan G. Global disease burden of COPD from 1990 to 2019 and prediction of future disease burden trend in China. *Public Health*. 2022;208:89–97. doi:10.1016/j.puhe.2022.04.015
8. Gondim FL, Moura MF, Ferreira RM, et al. Exposure to total particulate matter obtained from combustion of diesel vehicles (EURO 3 and EURO 5): effects on the respiratory systems of emphysematous mice. *Environ Toxicol Pharmacol*. 2021;83:103583. doi:10.1016/j.etap.2021.103583
9. Ferrera MC, Labaki WW, Han MK. Advances in chronic obstructive pulmonary disease. *Annu Rev Med*. 2021;72:119–134. doi:10.1146/annurev-med-080919-112707
10. Van Eeckhoutte HP, Donovan C, Kim RY, et al. RIPK1 kinase-dependent inflammation and cell death contribute to the pathogenesis of COPD. *Eur Respir J*. 2023;61(4):2201506. doi:10.1183/13993003.01506-2022
11. Ornatowski W, Lu Q, Yegambaram M, et al. Complex interplay between autophagy and oxidative stress in the development of pulmonary disease. *Redox Biol*. 2020;36:101679. doi:10.1016/j.redox.2020.101679
12. Dai Y, Zhang X, Ou Y, et al. Anoikis resistance--protagonists of breast cancer cells survive and metastasize after ECM detachment. *Cell Commun Signal*. 2023;21(1):190. doi:10.1186/s12964-023-01183-4
13. Paoli P, Giannoni E, Chiarugi P. Anoikis molecular pathways and its role in cancer progression. *Biochim Biophys Acta*. 2013;1833(12):3481–3498. doi:10.1016/j.bbamcr.2013.06.026
14. Haun F, Neumann S, Peintner L, et al. Identification of a novel anoikis signalling pathway using the fungal virulence factor gliotoxin. *Nat Commun*. 2018;9(1):3524. doi:10.1038/s41467-018-05850-w
15. Ma Z, Liu Z, Wu RF, Terada LS. p66(Shc) restrains Ras hyperactivation and suppresses metastatic behavior. *Oncogene*. 2010;29(41):5559–5567. doi:10.1038/onc.2010.326
16. Jang EJ, Sung JY, Yoo HE, et al. FAM188B downregulation sensitizes lung cancer cells to anoikis via EGFR downregulation and inhibits tumor metastasis in vivo. *Cancers*. 2021;13(2):247. doi:10.3390/cancers13020247
17. Yu Y, Song Y, Cheng L, et al. CircCEMIP promotes anoikis-resistance by enhancing protective autophagy in prostate cancer cells. *J Exp Clin Cancer Res*. 2022;41(1):188. doi:10.1186/s13046-022-02381-7

18. Li M, Zhang J, M Eng X, et al. Limb expression 1-like protein promotes epithelial-mesenchymal transition and epidermal growth factor receptor-tyrosine kinase inhibitor resistance via nucleolin-mediated ribosomal RNA synthesis in non-small cell lung cancer. *Cancer Sci*. 2023;114(4):1740–1756. doi:10.1111/cas.15687
19. Liao C, Li M, Chen X, et al. Anoikis resistance and immune escape mediated by Epstein-Barr virus-encoded latent membrane protein 1-induced stabilization of PGC-1α promotes invasion and metastasis of nasopharyngeal carcinoma. *J Exp Clin Cancer Res*. 2023;42(1):261. doi:10.1186/s13046-023-02835-6
20. Adeshakin FO, Adeshakin AO, Afolabi LO, Yan D, Zhang G, Wan X. Mechanisms for modulating anoikis resistance in cancer and the relevance of metabolic reprogramming. *Front Oncol*. 2021;11:626577. doi:10.3389/fonc.2021.626577
21. Wang LN, Zhang ZT, Wang L, et al. TGF-β1/SH2B3 axis regulates anoikis resistance and EMT of lung cancer cells by modulating JAK2/STAT3 and SHP2/Grb2 signaling pathways. *Cell Death Dis*. 2022;13(5):472. doi:10.1038/s41419-022-04890-x
22. Zhang C, Wang Y, Zhen Z, Li J, Su J, Wu C. mTORC1 mediates biphasic mechano-response to orchestrate adhesion-dependent cell growth and anoikis resistance. *Adv Sci*. 2024;11(6):e2307206. doi:10.1002/advs.202307206
23. Hu T, Mu C, Li Y, et al. GPS2 ameliorates cigarette smoking-induced pulmonary vascular remodeling by modulating the ras-Raf-ERK axis. *Respir Res*. 2024;25(1):210. doi:10.1186/s12931-024-02831-0
24. Entezari M, Taheriazam A, Orouei S, et al. LncRNA-miRNA axis in tumor progression and therapy response: an emphasis on molecular interactions and therapeutic interventions. *Biomed Pharmacother*. 2022;154:113609. doi:10.1016/j.biopha.2022.113609
25. Ma B, Wang S, Wu W, et al. Mechanisms of circRNA/lncRNA-miRNA interactions and applications in disease and drug research. *Biomed Pharmacother*. 2023;162:114672. doi:10.1016/j.biopha.2023.114672
26. Dong B, Gu Y, Sun X, et al. Targeting TUBB3 suppresses anoikis resistance and bone metastasis in prostate cancer. *Adv Healthc Mater*. 2024;13(28):e2400673. doi:10.1002/adhm.202400673
27. Tian T, Lu Y, Lin J, et al. CPT1A promotes anoikis resistance in esophageal squamous cell carcinoma via redox homeostasis. *Redox Biol*. 2022;58:102544. doi:10.1016/j.redox.2022.102544
28. Xu F, Vasilescu DM, Kinose D, et al. The molecular and cellular mechanisms associated with the destruction of terminal bronchioles in COPD. *Eur Respir J*. 2022;59(5):2101411. doi:10.1183/13993003.01411-2021
29. Fu G, Li ST, Jiang Z, et al. PGAM5 deacetylation mediated by SIRT2 facilitates lipid metabolism and liver cancer proliferation. *Acta Biochim Biophys Sin*. 2023;55(9):1370–1379. doi:10.3724/abbs.2023155
30. Zhang MX, Wang JL, Mo CQ, et al. CircME1 promotes aerobic glycolysis and sunitinib resistance of clear cell renal cell carcinoma through cis-regulation of ME1. *Oncogene*. 2022;41(33):3979–3990. doi:10.1038/s41388-022-02386-8
31. Ryan EM, Sadiku P, Coelho P, et al. NRF2 activation reprograms defects in oxidative metabolism to restore macrophage function in chronic obstructive pulmonary disease. *Am J Respir Crit Care Med*. 2023;207(8):998–1011. doi:10.1164/rccm.202203-0482OC
32. Masterson JC, Molloy EL, Gilbert JL, McCormack N, Adams A, O'Dea S. Bone morphogenetic protein signalling in airway epithelial cells during regeneration. *Cell Signal*. 2011;23(2):398–406. doi:10.1016/j.cellsig.2010.10.010
33. Zuo WL, Yang J, Strulovici-Barel Y, et al. Exaggerated BMP4 signalling alters human airway basal progenitor cell differentiation to cigarette smoking-related phenotypes. *Eur Respir J*. 2019;53(5):1702553. doi:10.1183/13993003.02553-2017
34. Zhang Y, Wang Y, Qian H. Multi-omics characterization and machine learning of lung adenocarcinoma molecular subtypes to guide precise chemotherapy and immunotherapy. *Front Immunol*. 2024;15:1497300. doi:10.3389/fimmu.2024.1497300
35. Cai K, Chen S, Zhu C, et al. FOXD1 facilitates pancreatic cancer cell proliferation, invasion, and metastasis by regulating GLUT1-mediated aerobic glycolysis. *Cell Death Dis*. 2022;13(9):765. doi:10.1038/s41419-022-05213-w
36. Pei Y, Lv S, Shi Y, et al. RAB21 controls autophagy and cellular energy homeostasis by regulating retromer-mediated recycling of SLC2A1/GLUT1. *Autophagy*. 2023;19(4):1070–1086. doi:10.1080/15548627.2022.2114271
37. Cho SJ, Moon JS, Nikahira K, et al. GLUT1-dependent glycolysis regulates exacerbation of fibrosis via AIM2 inflammasome activation. *Thorax*. 2020;75(3):227–236. doi:10.1136/thoraxjnl-2019-213571
38. Orsini EM, Roychowdhury S, Gangadhariah M, et al. TRPV4 Regulates the Macrophage Metabolic Response to Limit Sepsis-induced Lung Injury. *Am J Respir Cell Mol Biol*. 2024;70(6):457–467. doi:10.1165/rcmb.2023-0456OC
39. Mu C, Li Q, Niu Y, et al. Chronic diesel exhaust exposure induced pulmonary vascular remodeling a potential trajectory for traffic related pulmonary hypertension. *Respir Res*. 2024;25(1):348. doi:10.1186/s12931-024-02976-y
40. Liu H, Li J, Ma Q, et al. Chronic exposure to diesel exhaust may cause small airway wall thickening without lumen narrowing: a quantitative computerized tomography study in Chinese diesel engine testers. *Part Fibre Toxicol*. 2021;18(1):14. doi:10.1186/s12989-021-00406-1
41. Schmitt AM, Chang HY. Long Noncoding RNAs in Cancer Pathways. *Cancer Cell*. 2016;29(4):452–463. doi:10.1016/j.ccell.2016.03.010
42. Lu J, Kang X, Wang Z, Zhao G, Jiang B. The activity level of follicular helper T cells in the peripheral blood of osteosarcoma patients is associated with poor prognosis. *Bioengineered*. 2022;13(2):3751–3759. doi:10.1080/21655979.2022.2031387

Journal of Inflammation Research

Dovepress
Taylor & Francis Group

Publish your work in this journal

The Journal of Inflammation Research is an international, peer-reviewed open-access journal that welcomes laboratory and clinical findings on the molecular basis, cell biology and pharmacology of inflammation including original research, reviews, symposium reports, hypothesis formation and commentaries on: acute/chronic inflammation; mediators of inflammation; cellular processes; molecular mechanisms; pharmacology and novel anti-inflammatory drugs; clinical conditions involving inflammation. The manuscript management system is completely online and includes a very quick and fair peer-review system. Visit http://www.dovepress.com/testimonials.php to read real quotes from published authors.

Submit your manuscript here: https://www.dovepress.com/journal-of-inflammation-research-journal